4472–4485 *Nucleic Acids Research, 2016, Vol. 44, No. 9* *Published online 13 April 2016*
doi: 10.1093/nar/gkw231

Rapid generation of CRISPR/dCas9-regulated, orthogonally repressible hybrid T7-lac promoters for modular, tuneable control of metabolic pathway fluxes in *Escherichia coli*

Brady F. Cress[1], J. Andrew Jones[1], Daniel C. Kim[1], Quentin D. Leitz[1], Jacob A. Englaender[2], Shannon M. Collins[1], Robert J. Linhardt[1,2,3] and Mattheos A. G. Koffas[1,2,*]

[1]Department of Chemical and Biological Engineering, Center for Biotechnology and Interdisciplinary Studies, Rensselaer Polytechnic Institute, Troy, NY 12180, USA, [2]Department of Biological Sciences, Center for Biotechnology and Interdisciplinary Studies, Rensselaer Polytechnic Institute, Troy, NY 12180, USA and [3]Department of Chemistry and Chemical Biology, Center for Biotechnology and Interdisciplinary Studies, Rensselaer Polytechnic Institute, Troy, NY 12180, USA

Received January 24, 2016; Revised March 24, 2016; Accepted March 28, 2016

ABSTRACT

Robust gene circuit construction requires use of promoters exhibiting low crosstalk. Orthogonal promoters have been engineered utilizing an assortment of natural and synthetic transcription factors, but design of large orthogonal promoter-repressor sets is complicated, labor-intensive, and often results in unanticipated crosstalk. The specificity and ease of targeting the RNA-guided DNA-binding protein dCas9 to any 20 bp user-defined DNA sequence makes it a promising candidate for orthogonal promoter regulation. Here, we rapidly construct orthogonal variants of the classic T7-lac promoter using site-directed mutagenesis, generating a panel of inducible hybrid promoters regulated by both LacI and dCas9. Remarkably, orthogonality is mediated by only two to three nucleotide mismatches in a narrow window of the RNA:DNA hybrid, neighboring the protospacer adjacent motif. We demonstrate that, contrary to many reports, one PAM-proximal mismatch is insufficient to abolish dCas9-mediated repression, and we show for the first time that mismatch tolerance is a function of target copy number. Finally, these promoters were incorporated into the branched violacein biosynthetic pathway as dCas9-dependent switches capable of throttling and selectively redirecting carbon flux in *Escherichia coli*. We anticipate this strategy is relevant for any promoter and will be adopted for many applications at the interface of synthetic biology and metabolic engineering.

INTRODUCTION

Cells control gene expression with a variety of freely diffusing, natural transcriptional, translational, and post-translational control elements (1). Until recently, however, harnessing these regulators to engineer cells and design complex, layered genetic circuits has been complicated by the limited number of easily implemented and characterized orthogonal regulators, or regulatory parts that do not exhibit crosstalk. A particularly attractive control point for synthetic gene regulation is at the transcriptional level. If discrete ON/OFF transcription states can be maintained by a regulatory part (primarily mediated by low OFF state transcription or 'low-leakiness' during repression), then the added complexity of accounting for differential RNA accumulation, disparate translation rates, and other unforeseen factors at the translational and post-translational levels between circuit parts can be reduced or even neglected. Natural and synthetic transcription factors (sTFs) have been successfully applied to repress transcription from a promoter of interest in the context of increasingly complex genetic circuits. However, unanticipated interactions between transcriptional regulators and a non-cognate operator site—another transcriptional regulator's cognate operator—are problematic from a design perspective because they can lead to the unpredictable behavior of a synthetic genetic circuit composed of interconnected and layered parts. Thus, a core tenet of robust gene circuit design is the utilization of independent orthogonal control elements (including promoters and transcription factors) to improve predictability of a genetic circuit in disparate environments or contexts.

*To whom correspondence should be addressed. Tel: +1 518 276 2220; Fax: +1 518 276 3405; Email: koffam@rpi.edu

Impressive work, particularly that performed in the past five years, has attempted to address this problem by characterizing and refactoring natural and synthetic orthogonal regulators. Characterization in a cellular context includes quantification of at least two metrics:

1. The repressor dynamic range is the ratio of reporter gene expression between the de-repressed state (in absence of the cognate repressor) and the repressed state (in presence of the cognate repressor).
2. The orthogonality is quantified as the ratio of repression fold achieved by a cognate repressor versus unintended repression caused by a non-cognate repressor, and this metric needs to be determined for each repressor against all non-cognate promoters in a library.

Two primary approaches are taken for construction of orthogonal transcriptional regulator libraries. First, the coupling of bioinformatics and DNA synthesis has enabled so-called 'part mining', where homologs of well-characterized natural transcription factors are scraped from sequence databases, synthesized as DNA parts, and characterized *in vivo* with respect to dynamic range and orthogonality. Alternatively, with the increased ease of engineering zinc finger proteins (ZFPs) and transcription activator-like effectors (TALEs) to bind a user-defined DNA sequence, orthogonally regulated promoters have been generated *de novo* by placing ZFP or TALE binding sequences in the vicinity of a target promoter to prevent RNA polymerase from promoter recognition or halt the progression of RNA polymerase during transcription elongation (commonly referred to as roadblocking) (2–4). However, ZFP and TALE repressors, also known as sTFs, exhibit high cross-reactivity, and significant effort is required to screen for a subset of orthogonal sTFs (5). The RNA-guided DNA-binding protein dCas9 is an excellent alternative candidate for construction of orthogonal promoter-repressor sets.

Although dCas9 has been used as a multiplexing master transcriptional repressor against disparate promoters for many applications (6–9), only a few very recent examples have demonstrated rational promoter refactoring to enable orthogonal dCas9-mediated transcriptional repression controlled by small guide RNA (sgRNA)-promoter sets (5,8,10). These strategies invoke the reasonable assumption that more mismatches between the RNA guide and DNA target sequence will decrease binding frequency and strength relative to a complementary RNA:DNA heteroduplex. In one iteration, an *Escherichia coli* σ_{70} promoter constitutively driven by RNAp was manually redesigned to create five promoters, each possessing a unique 13 bp sequence or 'sgRNA operator' between the -35 and -10 elements (5). In a second example, the strong promoter P_L from phage lambda and commonly engineered promoters P_{BAD}, P_{lac}, and P_{luxI} were refactored by placing a protospacer adjacent motif (PAM)-proximal 20 bp dCas9 operator either upstream of the -35 site or downstream of the transcriptional start site; dCas9 operators and cognate sgRNAs were computationally designed to increase mismatches between sgRNAs and non-cognate operator sequences, thus decreasing potential for crosstalk between non-cognate promoters (10). Another variation utilized three randomly designed sequences as operators for dCas9 binding to create a set of three orthogonal promoters (8). In all of these cases, orthogonality was mediated by *de novo* sequence design with the intention of maximizing mismatches between sgRNA and non-cognate dCas9-binding sequences.

In contrast, we sought to generate orthogonally regulated promoters by both exploring and exploiting a reported property of dCas9-mediated transcriptional repression. Specifically, it has been shown in several works (11–13) that a single nucleotide mismatch between guide RNA and target DNA significantly attenuates or even abolishes dCas9-mediated repression, especially if the mismatch occurs in the 10–12 nucleotide sequence proximal to the PAM (previously dubbed as the seed region) (14). In the prevailing model of dCas9-mediated RNA:DNA hybridization, deduced from guide RNA-dCas9 co-crystal structure in apo and DNA-bound states, nucleation of RNA:DNA heteroduplex annealing occurs at two solvent-exposed nucleotides at the PAM-proximal 3′ end of the RNA targeting sequence (also known as the spacer) (15). Therefore, we hypothesized that a small number of mismatches in this region immediately adjacent to the PAM, hereafter referred to as the PAM-proximal seed nucleation region (PPSNR), would be sufficient to mediate orthogonality by impeding hybridization nucleation. As described below, we show that two to three mismatched nucleotides in the PPSNR can abrogate crosstalk between otherwise identical target sites, indicating that the prevailing strategy of maximizing mismatches across the entire dCas9 binding site is not necessary and that a simpler strategy can be employed to engineer orthogonality. Moreover, we demonstrate that constraining random mutations to a short segment of contiguous nucleotides in the seed region—rather than across the entire 20 bp dCas9-binding site as done in other work—facilitates fast learning about how mismatch count and nucleotide identity affects repression attenuation.

Toward this objective, we present a method for rapid construction and characterization of orthogonal CRISPR spacer-promoter pair libraries based on a small number of site-directed mutagenesis-mediated mismatches in the PPSNR (Figure 1). The classic promoter $P_{T7\text{-}lac}$ was utilized as a platform due to the high specificity of T7 RNA polymerase for the consensus T7 promoter sequence and due to its orthogonality to prokaryotic and eukaryotic promoters and polymerases, permitting high transcription rates upon induction with IPTG. Furthermore, the T7 promoter is a frequently engineered promoter that has found biotechnological and metabolic engineering applications in a wide range of hosts, including diverse bacterial species, yeast, and even mammalian cells (16,17). Recently, our lab reported construction of a $P_{T7\text{-}lac}$ library for optimizing metabolic pathways using mutant promoters, with randomly mutated transcription strength-determining sequences, exhibiting a wide range of transcription rates (18). Additionally, we demonstrated that dCas9 can effectively silence transcription by occlusion of T7 RNA polymerase (RNAp) from its cognate consensus binding site sequence in $P_{T7\text{-}lac}$ (6). Using this system, we probe the limits of PPSNR mismatch-mediated dCas9 repressor orthogonality and expose a clear boundary separating well-behaved non-cognate interactions from those exhibiting significant crosstalk. For the

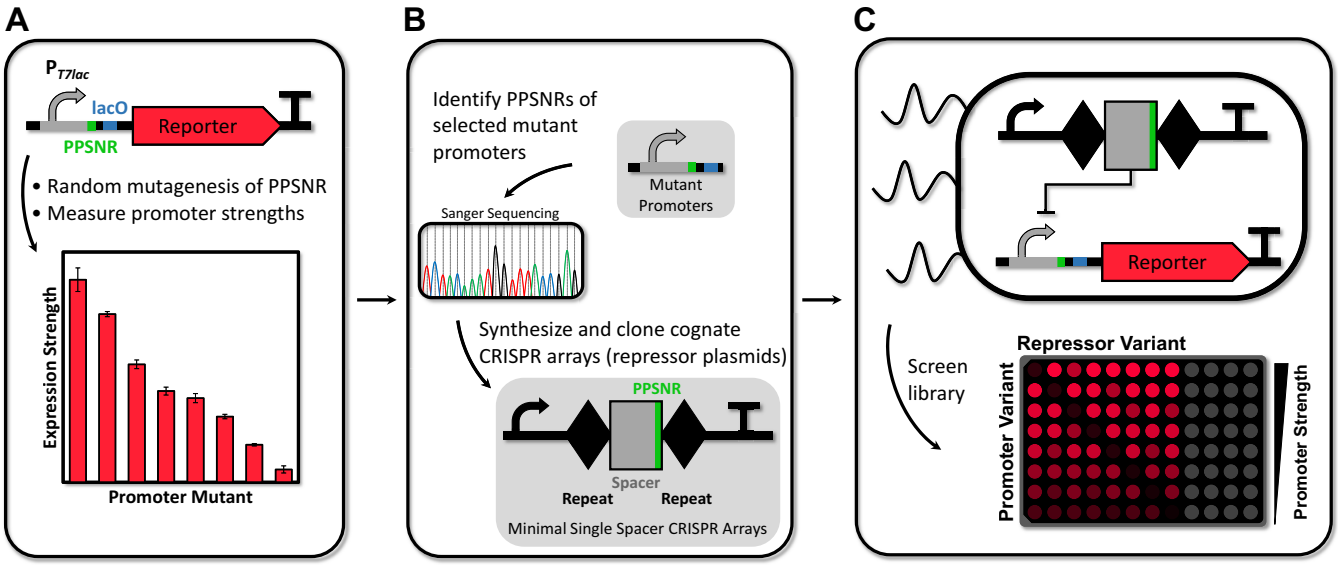

Figure 1. Pipeline for rapid generation and characterization of orthogonal dCas9-repressible promoter libraries. (**A**) Random mutagenesis of PPSNR (green) of protospacer (gray) near or within promoter (top) followed by promoter strength screen (bottom). (**B**) Select promoter mutants encompassing desired expression range (top), sequence selected promoters (middle), and construct cognate CRISPR-dCas9 repressor plasmids containing a single spacer CRISPR array (bottom). Sequences for promoters developed in this work are detailed in Figure 2A. (**C**) Co-transform reporter and repressor plasmid pairs (top) for combinatorial repression screen (bottom).

first time, we also show that crosstalk increases when number of target sites decrease, a property that reduces extensibility of minimally mismatched dCas9 repressor-promoter pairs but that could also be exploited as a design parameter. We believe that this critical discovery will have significant impact on *de novo* design of dCas9-based promoters in the future, because it illustrates that the context of a dCas9-based promoter (promoter copy number and number of competing sites relative to the intracellular concentration of dCas9) specifies the number of mismatches required to ensure orthogonality. Despite this important finding, we validate the utility of a well-behaved, orthogonal subset of minimally mismatched (only 2–3 bp) repressor-promoter pairs by using them as genetically encoded metabolic valves capable of orthogonally and dramatically redirecting metabolic flux at specified nodes in the highly branched five gene violacein biosynthetic pathway.

MATERIALS AND METHODS

Strain and plasmid construction

A promoter library was constructed by site-directed mutagenesis (QuikChange II, Agilent) of a high strength $P_{T7\text{-}lac}$ promoter variant from our previous work known as P_{C4} (18). Vector pETM6-C4-mCherry was used as a template to facilitate immediate screening of promoter strengths using *in vivo* fluorescence quantification (Figure 1A). Forward and reverse mutagenesis primers (IDT) were designed with four degenerate nucleotides overlapping part of the well-established transcription strength determining region of the consensus T7 promoter, a region conveniently situated immediately upstream of a PAM. PCR product was treated with DpnI (FastDigest, Thermo Scientific) to digest template plasmid prior to transformation into DH5α. Cells were plated on LB agar plates containing 80 μg/ml ampicillin and allowed to incubate at 37°C for 16 h. All colonies were scraped from the plate, and the mutagenized plasmid DNA library was harvested by miniprep of the pooled colonies. The library was then transformed into BL21 Star™ (DE3), and 276 individual colonies were inoculated into media for fluorescence assay as described below. Mutants covering a wide range of expression levels were selected for promoter sequencing, and those with identical sequences or unintended mutations were discarded. See Supplementary Table S1 for list of all plasmids constructed and utilized in this work, which have been made available to the community through Addgene (plasmids #73418-73440, 66530, 66533 and 66536).

Cognate CRISPR-dCas9 repressor plasmids (containing dCas9, tracrRNA, and a single spacer CRISPR array) for each corresponding promoter variant were constructed (Figure 1B) using Golden Gate assembly as described before (19). Two 35 bp complementary and slightly offset oligonucleotides (IDT) containing the spacer sequence for dCas9 targeting were phosphorylated with PNK (NEB) and annealed (37°C for 30 min, 98°C for 5 min, ramp down to 25°C over 15 min) to build inserts for each repressor variant. See Supplementary Table S2 for a list of all primers and oligonucleotides used in this work. Phosphorylated and annealed inserts were individually cloned into recipient plasmid pdCas9 (20) at two adjacent BsaI sites in the minimal, single-spacer CRISPR array using a one-pot Golden Gate reaction with BsaI (New England BioLabs) and T7 ligase (Epicentre Biotechnologies). Plasmid pdCas9 was a gift from Luciano Marraffini (Addgene plasmid # 46569). After confirmation by Sanger sequencing, chemically competent BL21 Star™ (DE3) containing each of 11 promoter variants driving mCherry expression

were prepared. Each of 12 CRISPR plasmids, 11 repressors plus the non-targeting (NT) spacer control plasmid pdCas9, was transformed into each individual mutant promoter strain, yielding a defined dual-plasmid strain library of 132 members (11 promoters × 12 CRISPR plasmids) as shown in Figure 1C. All 12 CRISPR plasmids were additionally transformed into *E. coli* JE1 harboring a single genomic copy of the $P_{T7\text{-}lac}$-mCherry cassette, and they were also co-transformed into MG1655 (DE3) (parent strain of JE1) with high copy plasmid pETM6-mCherry (ColE1 origin) possessing the same $P_{T7\text{-}lac}$-mCherry cassette for direct comparison of non-cognate repression of $P_{T7\text{-}lac}$ at different target copy number. Fluorescence quantification for every strain was performed as described in detail below.

Violacein pathway variants driven by orthogonal promoters developed in this work were constructed using the ePathBrick (21) restriction–ligation pathway cloning procedure as described in Supplementary Methods. Non-targeting spacer control plasmid pdCas9 and orthogonal repressors G6, 4A6, and 3A2 were individually co-transformed with each violacein pathway variant into BL21 Star™ (DE3). All cloning and plasmid maintenance was performed in DH5α. Cloning and site-directed mutagenesis were verified by Sanger sequencing, while ePathBrick subcloning was verified by restriction digestion. See Supplementary Table S3 for a list of all strains constructed in this work.

Fluorescence assay

Unless otherwise noted, all liquid cultures were incubated at 37°C and 250 rpm in 1 ml semi-rich defined media (AMM (6) supplemented with 2% glucose and appropriate antibiotics) in polypropylene 48 deep-well plates (5 ml, VWR) covered with breathable rayon film (VWR). Glycerol stocks of expression strains containing either a single reporter plasmid (promoter screening) or both a reporter plasmid (or genomic cassette) and a CRISPR-dCas9 repressor plasmid (repressor screening) were streaked onto LB agar plates containing appropriate antibiotics (80 μg/ml ampicillin and 25 μg/ml chloramphenicol as necessary). Individual colonies were inoculated into a single well of a polypropylene 48 deep well plate. Overnights were allowed to grow 14 h in a rotary shaker before subculturing at 1:50 dilution into fresh media in a new 48 deep well plate. Following 4 h of growth, cultures were induced near mid-log phase with 0.1 mM IPTG and grown under the same conditions overnight. Cognate repressor and non-targeting control strains were also grown for the same period of time without induction to check for leaky expression in absence of IPTG (Supplementary Figure S7). Endpoint mCherry fluorescence (excitation wavelength of 588 nm and emission wavelength of 618 nm) and OD650 measurements were obtained in 96-well black clear bottom plates (Nunc Products) on a Biotek Synergy 4 instrument 20 h post-induction (Supplementary Table S4 and Supplementary Figure S1). Cultures were diluted into the linear range as necessary. Endpoint fluorescence quantification experiments were reproduced in four independent experiments on different days. Transient post-induction expression data obtained for all cognate repressor and non-targeting control strains is shown in Supplementary Figure S6. Qualitative endpoint fluorescence images of mCherry from liquid cultures (experiment performed on fifth independent day) were taken in either 96- or 384-well black clear bottom plates (Nunc Products) on a Typhoon Trio Plus Imager flatbed scanner (GE Healthcare) with excitation at 532 nm (green laser) and emission filter set to 610 nm bandpass (610 BP 30).

Violacein pathway metabolite production and quantification

Violacein production and quantification were performed as recently described by our lab (18). Briefly, BL21 Star™ (DE3) glycerol stocks containing both a violacein pathway variant and a CRISPR repressor plasmid or negative control repressor plasmid (G6, 4A6, 3A2 or NT) were streaked onto LB agar plates containing appropriate antibiotics. Individual colonies were inoculated into 48 deep well plates and grown overnight for 14 h, when they were subcultured at 1:50 dilution into 2 ml fresh media. At 3.5 h post-inoculation, the temperature was reduced from 37°C to 20°C to allow cultures to acclimate prior to induction with 1 mM IPTG at 4.5 h post-inoculation. Each strain was assessed in biological triplicate, and cultures were sampled at 16 hours post-induction. Aliquots (1.5 ml) of each culture were centrifuged for 5 min at 21 000 × g and supernatant was removed to quantify the fold changes of violacein and the pathway side-products in cell pellets. Cell pellets were then extracted by addition of 500 μL methanol containing 1% (v/v) acetic acid, followed by brief vortexing and boiling for 5 min. Cell debris was pelleted by centrifugation at 21 000 × g for 10 min, and extracts were analyzed as previously reported by our lab (18) using an Agilent 1200 series HPLC equipped with a ZORBAX SB-C18 StableBond analytical column (150 mm × 5 mm, 5 μm) maintained at 30 °C and a diode array detector (DAD). Mobile phase A was acetonitrile and mobile phase B was water (both containing 0.1% formic acid). The following gradient was used at a flow rate of 1 ml/min: 0 min, 5% A; 1 min, 5% A; 5 min, 45% A; 7 min, 55% A; 9 min, 95% A; 10 min, 5% A; 12 min, 5% A. Proviolacein (7.1 min), prodeoxyviolacein (7.8 min), violacein (8.1 min) and deoxyviolacein (9.3 min) were analyzed by peak area integration at 600, 610, 565 and 565 nm, respectively. Injection volume was 50 μl and was adjusted as necessary to fall within the linear response range of the assay.

RESULTS AND DISCUSSION

Generation of dCas9-repressible $P_{T7\text{-}lac}$ library using site-directed mutagenesis

Site-directed mutagenesis was performed on the first four nucleotides of the 5 bp transcription strength-determining region of the T7 promoter to create a panel of useful $P_{T7\text{-}lac}$ variants covering a wide range of transcriptional strengths. Mutations in this 5 bp motif have been shown to dramatically alter transcriptional strength without altering T7 RNA polymerase specificity toward the promoter, a property that is instead controlled by a 6 bp sequence upstream of the strength-determining region (Figure 2A) (22,23). The four randomized nucleotides were selected because they also correspond to critical elements required for

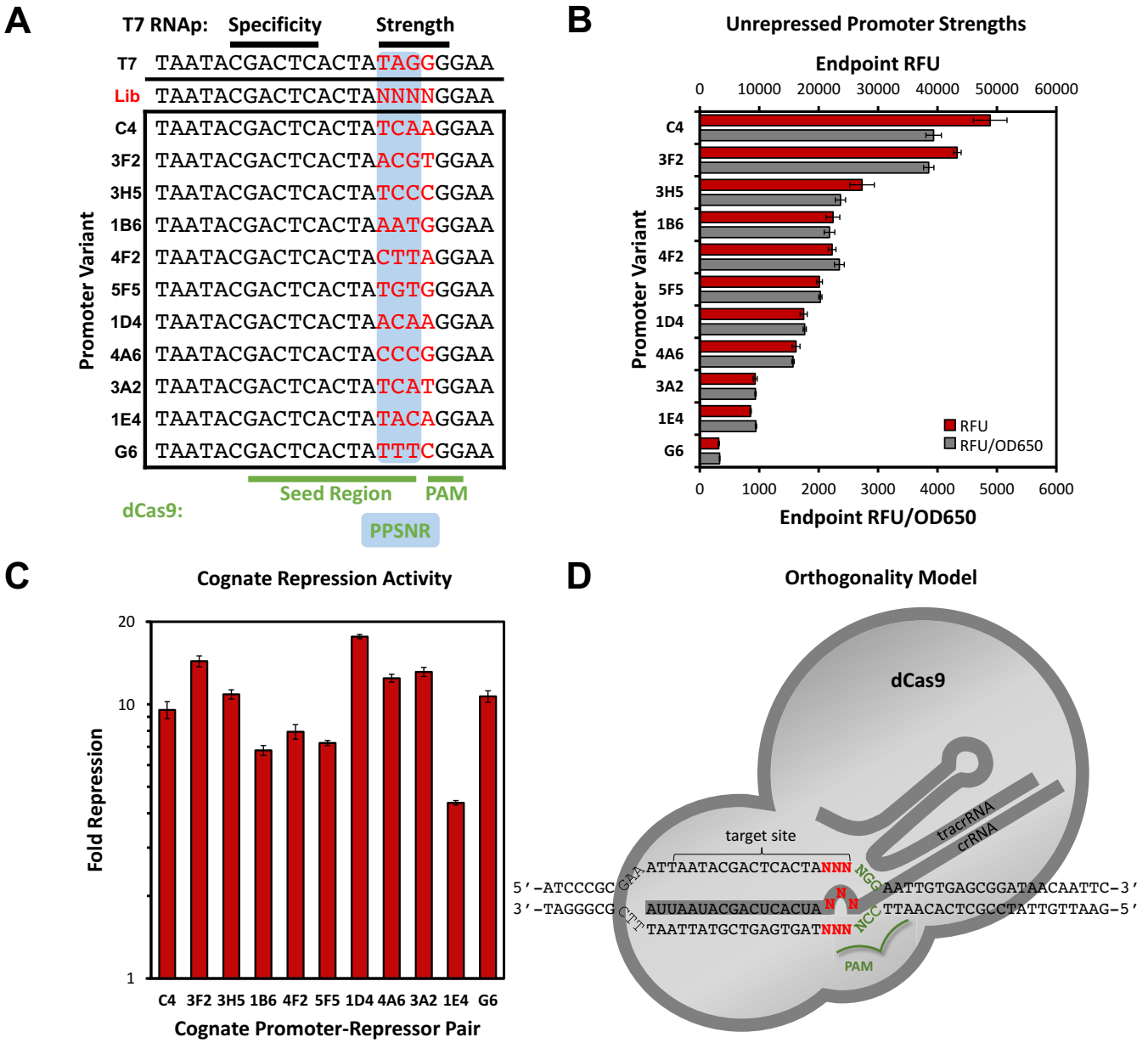

Figure 2. Hybrid promoter library design. (**A**) Site-directed mutagenesis of four nucleotides (red) was used to construct a randomized library of classic promoter $P_{T7\text{-}lac}$ (top) variants (bottom), each with different transcription strengths. Sequences affecting T7 RNAp specificity and strength (black, top); sequences mediating dCas9 binding (green, bottom) and orthogonality (blue). (**B**) Expression strengths of selected unrepressed promoter mutants in absence of cognate repressor but in presence of dCas9, tracrRNA, and a non-targeting crRNA control. (**C**) Endpoint fold repression of cognate dCas9 repressors relative to the non-targeting control repressor. (**D**) Schematic representation of dCas9-binding and orthogonality model. PPSNR hybridizations for the defined library are shown in Supplementary Table S8. All measurements were performed in four independent experiments on different days ($n = 4$). Values represent mean endpoint expression level or endpoint repression percentage relative to the non-targeting repressor control strain, and error bars represent SEM.

dCas9-targeting. As seen in Figure 2A, a conveniently situated PAM-proximal protospacer (dCas9 target) exists in the consensus $P_{T7\text{-}lac}$ sequence, spanning both the transcription rate-determining region and the transcriptional start site. The first three mutagenized nucleotides correspond to the three bp PPSNR, while the fourth mutagenized nucleotide should not affect orthogonality since it constitutes the first base pair of the PAM, a region not involved in base-pairing during dCas9-mediated RNA:DNA hybridization (Figure 2D). Thus, randomization of this precise four bp sequence facilitates control of two important parameters, the maximum expression level of distinct promoter variants in the absence of LacI/dCas9 (unrepressed state) and the orthogonality between promoter variants in the presence of dCas9 (repressed state).

Transcription strengths of promoter variants were initially screened by quantification of mCherry fluorescence in the absence of dCas9, and a subset of 11 promoters, includ-

ing two from our previous work (P_{C4} and P_{G6}), covering an expression (fluorescence normalized by cell density) range of >10-fold were selected for repression studies (Figure 2B). In future applications, the wide expression range spanned by this defined library will facilitate transcriptional balancing within a genetic circuit through random screening or rational selection of promoter mutants with known strengths in a manner akin to recent efforts in metabolic pathway balancing (18,24). While some high-strength promoter variants developed here could potentially cause metabolic burden in the host cell (P_{C4} and P_{3F2}, for instance) (25), promoter choice will ultimately be guided by a user's intended application.

Importantly, the benefit of utilizing dual regulators in this hybrid promoter architecture is two-fold. First, LacI is used as a master repressor that permits coordinated transcription across all promoter variants upon addition of a single external inducer, IPTG, an important feature for metabolic engineering when production capacity of a biosynthetic pathway is highly sensitive to induction timing. Second, since dCas9-mediated repression has been shown to be non-cooperative (5), use of the cooperative repressor LacI prevents leakiness in its bound (repressed) state, while dCas9 acts as a slightly leaky (Supplementary Figure S7) but highly selective multiplexing repressor. Future efforts to engineer cooperativity for dCas9-mediated transcriptional repression in prokaryotes could reduce this leakiness and could obviate the need for a dual regulatory architecture when coordinated induction across many promoters is not required.

Quantitative measurement of dCas9-mediated transcriptional repression activity

Combinatorial repression activity assays were performed for 11 spacer sequences against all cognate (perfectly complementary) and non-cognate (mismatched) promoters to generate what we hereby define as a CRISPoRthogonality matrix, tabulating the endpoint repression percentage achieved in 121 (11^2) defined strains relative to 11 non-targeted control strains (Figure 3B). A fluorescence image of the 121 member library is shown in Figure 3A. Promoter-repressor pairs are notated in this work as R_x:P_y, or repressor x against promoter y. As expected, all repressors exhibited significant repression against their cognate promoters, R_x:P_x, with a dynamic range of greater than 10-fold on average and up to 15-fold for some cognate promoter-repressor pairs (Figure 2C and Supplementary Table S6). Contrary to observations in other works, however, some spacers exhibited substantial repression against mismatched, non-cognate promoters, especially those possessing only a single mismatch (Figure 3C).

A single mismatch in the PPSNR is not sufficient to abolish dCas9-mediated repression

A common inference from CRISPRi mismatch studies has been that a single mismatch is sufficient to significantly attenuate or abolish dCas9-mediated repression (8,11–13). However, the existence of well-documented off-target effects, or the ability of Cas9 to cut slightly mismatched targets such as those containing indels relative to the guiding RNA sequence (26–28), indicates that Cas9 tolerates mismatches to some unknown extent. Despite this knowledge, it was surprising to measure dramatic repression for a substantial proportion of non-cognate interactions—often within 20% of cognate repression, and sometimes equivalent—as seen in the CRISPoRthogonality matrix in Figure 3. Since theoretical models for predicting the effect of mismatches on dCas9-mediated hybridization and subsequent transcriptional repression activity are nascent (29,30), we explored factors that could potentially explain strength of non-cognate repression. First, we expected that high non-cognate repression was likely enabled by tolerance for a low number of mismatches and posited that an inverse relationship might exist between number of mismatches and repression activity. This notion is supported by the qualitative symmetry of repression activity across the diagonal of the CRISPoRthogonality matrix as seen in Figure 3B and the fact that a corresponding matrix tallying the number of PPSNR mismatches (Supplementary Table S9) is symmetric, (R_x:P_y and R_y:P_x share the same number of mismatches). Indeed, it can be discerned by comparison of Figure 3B and C that promoter-repressor pairs with 0–1 mismatches exhibit the highest repression and that, in general, the number of mismatches between CRISPR RNA and target DNA is a good qualitative predictor for the existence of non-cognate repression in our system. Perhaps unexpectedly, repression activity is not well correlated between matched off-diagonal pairs (e.g. R_{C4}:P_{1D4} versus R_{1D4}:P_{C4}) in the case of single mismatches (1 mm) that achieve intermediate repression levels, but the inverse relationship between number of mismatches and repression activity can be visualized in Figure 4A by the movement of clusters toward the origin as mismatch number increases. When all promoter-repressor pairs are grouped by number of mismatches, ratios of mean repression fold between 0 mm and 1 mm pairs (∼2×) and between 1 and 2 mm pairs (∼5×) are statistically significant (Figure 4B). Conversely, ratio of mean repression fold between 2 and 3 mm pairs is statistically indistinguishable. Another point that should not be discounted is that, as demonstrated in Figure 4A, single mismatches in the PPSNR can achieve a wide range of repression activities (∼30–90%) and could be used to tune transcription strength *in trans* (and even dynamically) as a complement to traditional promoter strength tuning achieved through promoter mutagenesis.

Given the wide distribution of repression levels achieved by non-cognate pairs, we also attempted to infer the effect of several factors on mismatch tolerance. In this dataset, mismatch configuration, or position ignoring nucleotide identities, was not sufficient to explain mismatch tolerance (Supplementary Figure S2). Furthermore, as certain mismatches have been shown to stabilize DNA:DNA (31), RNA:RNA (32) and even RNA:DNA (33,34) duplexes, the effect of nucleotide pair identity on mismatch tolerance was also assessed by considering only single mismatch cases in order to preclude interaction effects stemming from more than one mismatch that could otherwise confound inferences. In this dataset, single rU•dC/rC•dT mismatches were found to attenuate repression fold change ∼3.1× relative to other single mismatch types, while rU•dT (rU•rU in RNA duplexes are stabilizing in some cases (32)) and

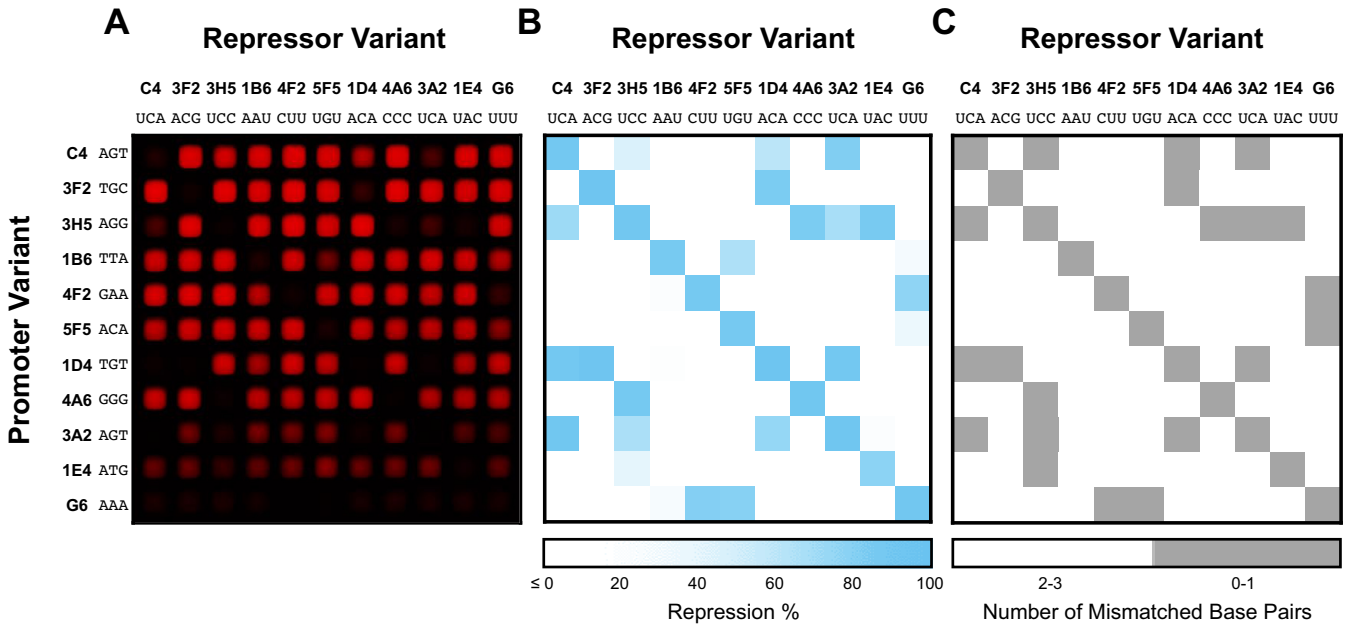

Figure 3. CRISPoRthogonality matrix. (**A**) Fluorescence image of *Escherichia coli* cultures expressing mCherry from representative repression activity experiment. Strains harboring cognate promoter-repressor pairs are seen on the diagonal from upper left to lower right, and non-cognate pairs on the off-diagonal. 3 bp nucleotide sequences of 5′ to 3′ RNA PPSNR (top) and 3′ to 5′ DNA complement PPSNR (left) are shown. (**B**) Endpoint repression activity presented as percent repression relative to non-targeting repressor control strain possessing the same promoter variant. Non-cognate repression is seen in many cases but appears qualitatively symmetric (R_x:P_y repression activity suggests the presence of R_y:P_x repression activity). (**C**) Number of mismatches between repressor RNA and target DNA, where the presence of 0–1 mismatches (gray) leads to high repression relative to the presence of two to three mismatches (white). Values represent mean of measurements performed in four independent experiments on different days ($n = 4$). Mean and SEM values are tabulated in Supplementary Table S5.

rT•dG/rU•dG (wobble base pair) mismatches were found to increase repression fold change approximately 2.5× relative to other mismatch types (Supplementary Figure S3); despite the statistical significance found here, we caution that these results should not be interpreted as general design rules until larger sample sizes are assessed against diverse target sequences, especially because mismatch stability is often dependent upon position in a duplex and identity of neighboring nucleotides. Finally, while reconciliation of repression data with theoretical predictions of dCas9:RNA:DNA stability (free energy of dCas9-mediated formation of an R-loop, or the three-stranded structure composed of the RNA:DNA hybrid and the displaced ssDNA complement) is tempting, there is a dearth of structural and thermodynamic data impeding accurate prediction of mismatched RNA:DNA hybridization free energy. Although stabilities of RNA:DNA heteroduplexes exclusively composed of Watson-Crick base-pairs and a few mismatch types are known, prediction of hybridization free energy for RNA:DNA heteroduplexes with loops (bulges and mismatches), non-Watson–Crick base pairs (wobble or other non-canonical pairs), and terminal mismatches is an open problem (35). If these data were abundant, however, we speculate that a model of RNA:DNA hybridization free energy accounting for these factors might be used to better predict R-loop stability and thereby dCas9-mediated repression activities (29). In summary, the best predictor of repression strength inferred from this dataset is number of mismatches, where a clear boundary between high and low repression is established between one and two PPSNR mismatches, respectively, and three PPSNR mismatches are sufficient to abrogate dCas9-mediated transcriptional repression in the specified context.

Target copy number affects mismatch tolerance

Synthetic parts are commonly moved between the genome and plasmids with different replication origins of defined copy number to facilitate construction of genetic circuits. As reported frequently in recent years, this strategy effectively alters part response by titrating part copy number relative to other interacting parts, culminating in undesirable gene circuit dynamics (36–38). Therefore truly robust parts are those that exhibit similar characteristics (or response curves) when expressed at distinct copy numbers, for instance, when moved from a single copy in the genome to a very high copy plasmid. Until a generally applicable method has been developed to stabilize performance of any part between different expression contexts (an impressive feat that could be considered a grand challenge of synthetic biology), it is instructive to investigate the effect of altered copy number on newly designed parts. In previous work, we have shown that cognate repression fold change increases 1 to 2 orders of magnitude (64x) against a genome-based $P_{T7\text{-}lac}$-mCherry cassette (one copy) relative to an identical plasmid-based cassette (ColE1 origin, ∼40 copies), suggesting that dCas9 or targeting RNA is limiting when target copy number is high (6). Therefore, in an effort to understand if the minimum number of mismatches necessary to abrogate repression changes with target copy number,

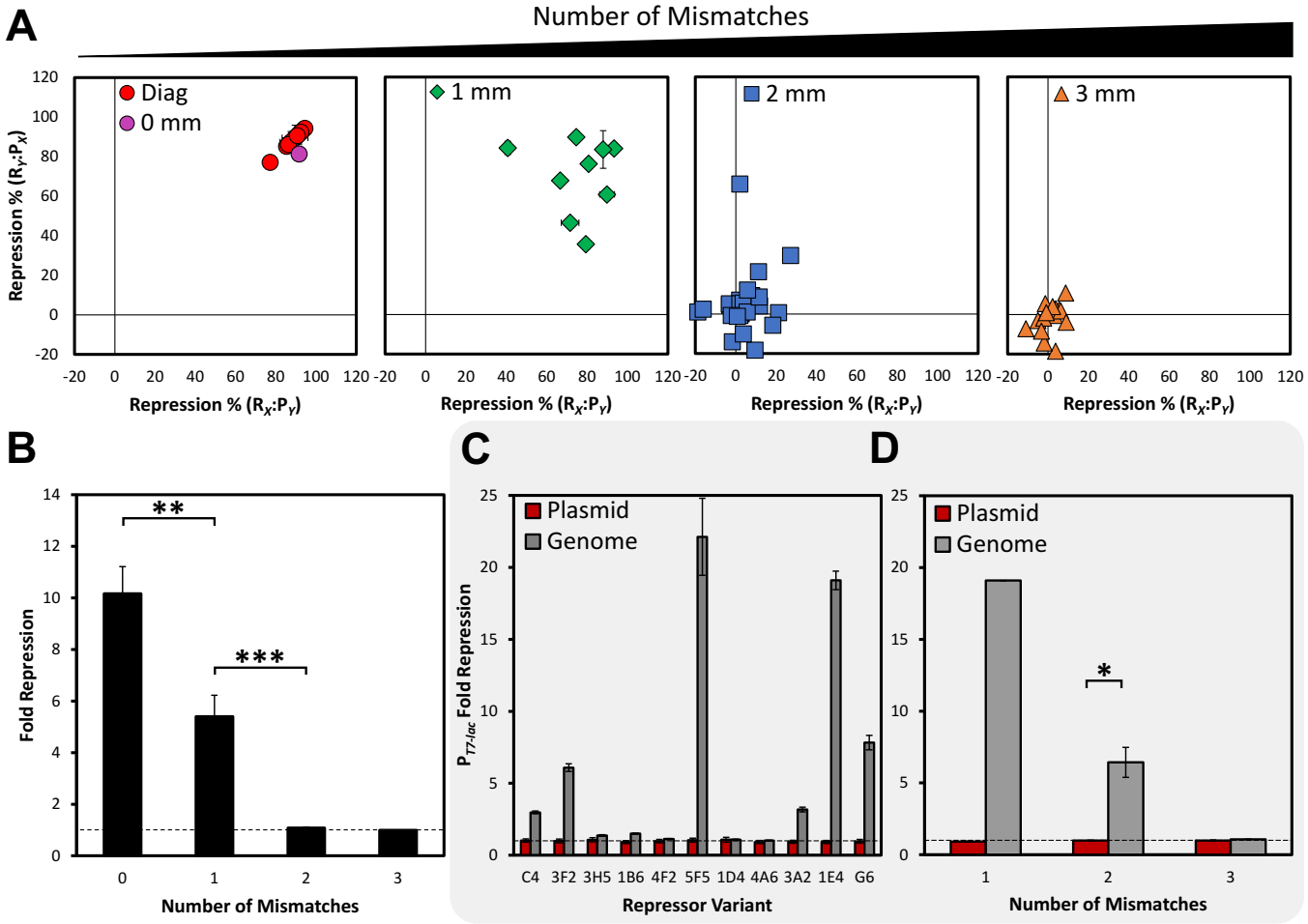

Figure 4. Effect of mismatches on repression activity. (**A**) Endpoint repression percentage by mismatch count. Each point represents cross-part repression for a two part subset (R_X:P_Y on one axis and its inverse pair R_Y:P_X on the other). Cognate interactions with 0 mm (red circles) include subset [C4 3A2] (purple circle, no PPSNR mismatches but possesses distinct nucleotide in first base of PAM). Mismatch number increases from left to right: 1 mm (green diamonds), 2 mm (blue squares), and 3 mm (orange triangles). Measurements performed in four independent experiments on different days ($n = 4$), and error bars show SEM. (**B**) Pooled data from (**A**). Mean fold change ratios are highly significant between 0 mm to 1 mm (1.9×, ** $\alpha < 0.01$) and between 1 and 2 mm (5×, *** $\alpha < 0.001$), while repression activity between 2 mm and 3 mm is statistically indistinguishable (one-way Welch's ANOVA, Games-Howell *post-hoc* comparison for unequal sample sizes and variances). Values represent mean fold repression from all tested pairs grouped by 0, 1, 2 and 3 mismatches ($n = 13$, 18, 54 and 36, respectively), and error bars represent SEM. (**C**) Fold repression of non-cognate repressors against consensus $P_{T7\text{-}lac}$–mCherry expression cassette harbored on plasmid (red) or genome (gray). Values are mean of five independent biological replicates ($n = 5$), and error bars represent SEM. (**D**) Data from (**C**) pooled by number of mismatches. Mean fold change ratio of ∼6.5× for 2 mm repressors against same target at different copy numbers is statistically significant (* one-tailed *t*-test with Welch's correction for unequal variances, $P = 0.048$), while statistically indistinguishable for 3 mm repressors. Fold repression ratio of ∼21× is seen for the only 1 mm repressor assessed against $P_{T7\text{-}lac}$; however, sample size is too low ($n = 1$) to make general inferences. Values are mean fold change of repressors grouped by 1, 2 or 3 mm ($n = 1$, 7 and 3, respectively), and error bars represent SEM.

we compared repression activity of all non-cognate repressors against this genome-based and plasmid-based $P_{T7\text{-}lac}$-mCherry cassette. As seen in Figure 4C, some non-cognate repressors showed very high repression activity against the single genomic reporter compared to the reporter plasmid. After pooling the non-cognate repression activities by number of mismatches, it is apparent that repression strength increases with decreasing number of mismatches, and that the boundary separating high and low activity non-cognate repressors against the single genomic target exists between two and three mismatches (Figure 4D) as compared to one and two mismatches for the average plasmid-based target (Figure 4B). This represents an increase in tolerance of at least one additional PPSNR mismatch against a single copy target compared to a high copy target. Although rules governing this shift in mismatch tolerance should be further investigated, this important first indication that mismatch tolerance is a function of target copy number suggests that mismatch number is critical for tuning orthogonality between similar promoters in different expression contexts.

Quantification of orthogonality within part subsets

Although non-orthogonal interactions were uncovered throughout the library, several subsets with high average orthogonality (mean of all non-cognate orthogonality values) can be ascertained. We quantify orthogonality of each promoter-repressor interaction in the full library (Supplementary Table S7), and we illustrate that selection of appro-

priate promoter–repressor subsets simply through manual inspection improves mean orthogonality while simultaneously reducing orthogonality variance amongst the subset relative to the full set (subset [C4 3F2 1B6 4F2] in Figure 5C). Minimum orthogonality—fold change between on-target effect against a part and the strongest off-target effect observed for that part within the subset, also referred to as orthogonal range (39)—is also higher for many subsets relative to the full set. Compared to average orthogonality, minimum orthogonality is a critical metric for selecting well-behaved parts subsets, because it ensures that individual parts otherwise contributing to high average orthogonality are ranked low if even a single unintended interaction is detected that could lead to undesired crosstalk in a genetic circuit. Systematically assessing and ranking all possible subset combinations of all possible subset sizes by minimum orthogonality threshold (Figure 5A), we find 10 subsets of three promoter-repressor pairs and two subsets of four promoter-repressor pairs exhibiting a minimum orthogonality of 8x, all of which possess a mean orthogonality of 11–14× (Figure 5B, Supplementary Table S10, and Supplementary Figure S4).

While we note that other work, including our own (6), has demonstrated greater dynamic range of dCas9-mediated repression (which augments orthogonal range) in certain contexts, particularly against low-copy target sites, we stress that there are trade-offs between dynamic range, orthogonality, toxicity, and intended application of transcription factors (40). Specifically, we suspect that increased expression of dCas9 or guide RNA (crRNA and tracrRNA in this system) might improve repression dynamic range against the T7 promoter and any strong promoter on a high copy plasmid with a trade-off of introducing toxicity or growth burden during overexpression of dCas9 and other CRISPR elements as previously described elsewhere (5). Alternatively, if dCas9 could be engineered to act as a cooperative DNA-binding protein like natural transcription factors, higher repression activity could likely be attained with lower expression of dCas9 and other CRISPR elements, reducing the negative effects of dCas9 overexpression on cell growth. To frame our work, a recently published example of engineered dCas9-based repressors against P_{BAD}, P_{lac}, and P_{luxI} achieved similar repression levels to this effort, and this level was adequate to generate functional double and triple inverter circuits (10). Therefore, given our interest in development of practical tools at the interface of synthetic biology and metabolic engineering (41), we opted to showcase the remarkable functionality and extraordinary orthogonality of these minimally-mismatched dCas9 repressor-promoter sets in *E. coli* by implementing facile control over the flow of carbon toward several distinct, brilliantly colored metabolites in the violacein pathway.

Orthogonal hybrid dCas9-T7-lac promoters act as independent metabolic switches

The five gene violacein pathway (Figure 6B and Supplementary Figure S8) is becoming a valuable model pathway for proof-of-principle demonstrations of tools at the interface of synthetic biology and metabolic engineering (7,42–45) due to its exceedingly branched nature and ap-

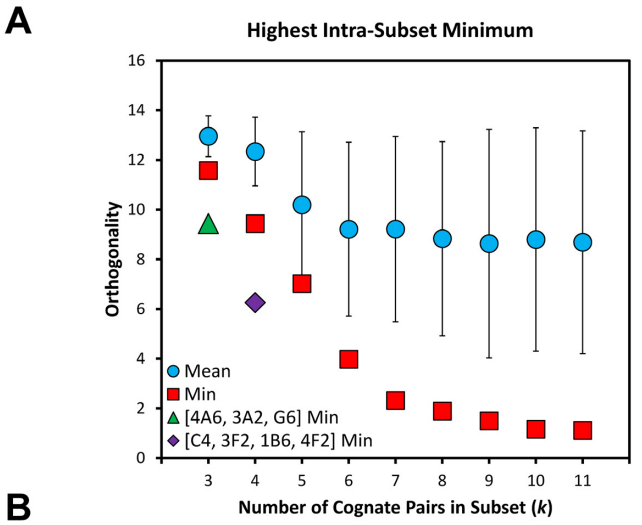

B

Size of Largest Tested Parts Set Meeting Orthogonality Criteria

Orthogonality Criteria (combinations)		Cognate Pairs in Subset (*k*) 3 (165)	4 (330)	5 (462)	6 (462)	7 (330)
Min >	10x	5	-	-	-	-
	8x	10	2	-	-	-
	6x	46	24	4	-	-
	4x	61	39	8	6	-
Mean >	13x	3	-	-	-	-
	12x	10	1	-	-	-
	11x	27	20	2	-	-
	10x	43	72	68	25	5
Subset with Highest Minimum Orthogonality	Mean	13.0x	12.3x	10.2x	9.2x	9.2x
	SD	0.8	1.4	3.0	3.5	3.7
	CV	6.4%	11%	29%	38%	40%
	Min	11.6x	9.4x	7.0x	4.0x	2.3x

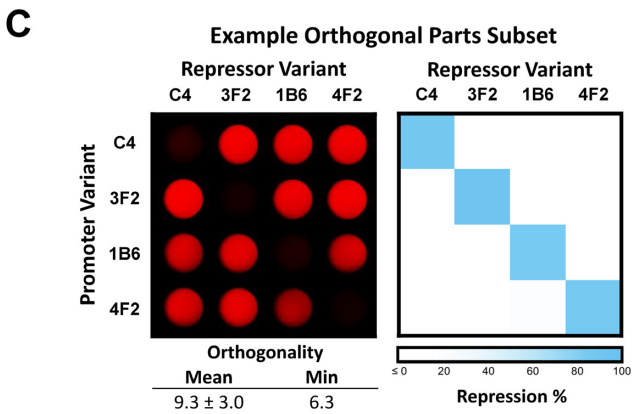

Figure 5. Orthogonal subset analysis. (**A**) Orthogonality metrics for 'best' subset (possessing highest minimum orthogonality) of each subset size (k) from the full set of cognate promoter-repressor pairs ($n = 11$). Symbols represent mean orthogonality (blue circles), minimum orthogonality of best subset (red squares), and minimum orthogonality of two parts subsets (green triangle and purple diamond) further used in this work. (**B**) Tabulation of distinct parts sets of stated size meeting specified orthogonality criteria (top) and orthogonality metrics for the best subset within each subset size (bottom, $k = 3$–7). (**C**) Subset [C4, 3F2, 1B6, 4F2] (purple diamond in **A**) with mean orthogonality of 9.3 and minimum orthogonality of 6.3 is highlighted as an example subset with high average unrepressed promoter strength. In this case, minimum orthogonality (strongest non-cognate effect in the subset) is set by the interaction between P_{4F2} and R_{1B6}.

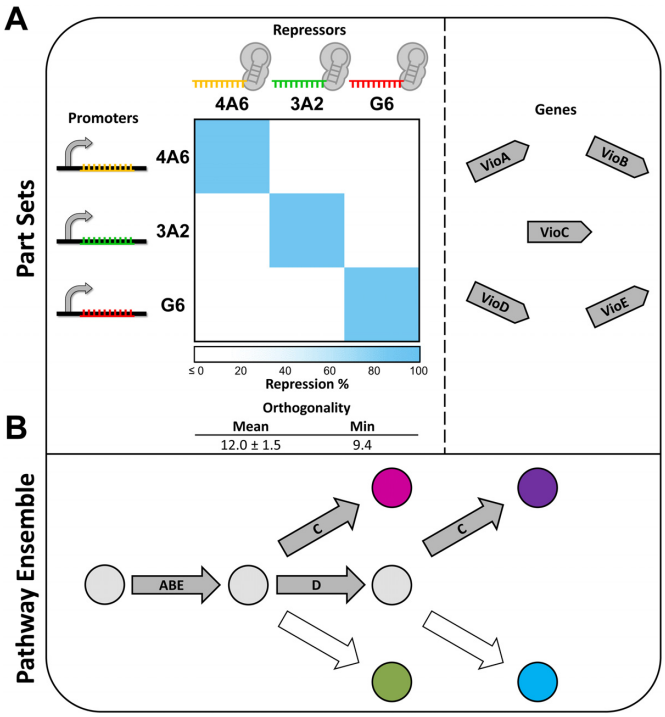

Figure 6. (**A**) The parts set used in this work includes three orthogonal hybrid promoters with minimum orthogonality of ∼10×, three dCas9 sTFs R_{G6} (red), R_{4A6} (yellow), R_{3A2} (green), and five violacein biosynthetic genes VioABCDE (gray) were used to construct four pathway variants, each possessing orthogonal promoters at carefully selected nodes in the branched violacein pathway. (**B**) Ensemble of the violacein biosynthetic pathways and metabolites. Colored nodes represent the major violacein pathway metabolites prodeoxyviolacein (olive green), proviolacein (cyan), deoxyviolacein (pink) and violacein (violet), while gray nodes represent precursor and intermediate metabolites.

titude for simultaneous high level production of multiple distinctly colored metabolites. Accordingly, an orthogonal subset of refactored promoters developed in this work (P_{G6}, P_{4A6} and P_{3A2}) were incorporated into key nodes in the violacein biosynthetic pathway to demonstrate their ability to act as dCas9-dependent valves capable of throttling or selectively redirecting carbon flux, and the entire set of parts utilized in this system are shown in Figure 6A. The following four pathway variants were constructed using ePathBrick (21) in monocistronic configuration, where transcription of each gene is driven by one of the aforementioned dedicated $P_{T7\text{-}lac\text{-}dCas9}$ hybrid promoters and terminated with the classic T7 terminator.

1. pETM6-G6-VioABE
2. pETM6-G6-VioABECD
3. pETM6-G6-VioABE-4A6-VioC
4. pETM6-G6-VioABE-4A6-VioC-3A2-VioD

Pathway variants 1 and 2, driven entirely by P_{G6}, were constructed to illustrate orthogonality of the G6 promoter to non-cognate R_{4A6} and R_{3A2} at the level of metabolite production. As seen in Figure 7A and B, the final product of the three-gene VioABE pathway, prodeoxyviolacein (green), is repressed by the cognate G6 repressor ∼40-fold compared to the non-targeting control strain. Critically, R_{4A6} and R_{3A2} do not exhibit repression of prodeoxyviolacein production in this system. Furthermore, the major products of the full pathway P_{G6}-VioABECD, violacein (purple), deoxyviolacein (reddish-purple), and proviolacein (bluish-purple), are repressed by the cognate repressor R_{G6} ∼10- to 20-fold compared to the non-targeting control strain. Similarly, high-capacity production of these three major products is retained in the P_{G6}-driven pathway despite the presence of R_{4A6} and R_{3A2} (Figure 7C and D). It should be noted that prodeoxyviolacein was not detected by HPLC in either of the cultures expressing VioD, possibly due to decreased accumulation of the intermediate protodeoxyviolaceinic acid in presence of two enzymes (VioC and VioD), which would likely hamper spontaneous (non-enzymatic) flux toward prodeoxyviolacein.

Pathway variants incorporating distinct promoters were constructed to demonstrate that orthogonal dCas9 promoters can be utilized as independent metabolic switches. Pathway variant 3 consists of *vioABE* driven by P_{G6} and a genetically encoded switch, *vioC* driven by P_{4A6}, yielding metabolites deoxyviolacein and prodeoxyviolacein when not repressed. As seen in Figure 8A and B, repression of the committed gene *vioA* and the following two genes, *vioBE*, with R_{G6} leads to nearly complete repression of both metabolites as visualized by the neutral culture color and by HPLC analysis. Additionally, carbon flux diversion in this pathway yields a visually striking color difference (from reddish-purple to green) when the R_{4A6} switch is used to shunt flux from deoxyviolacein (80% decrease) to prodeoxyviolacein (440% increase). The dramatic color differences between these cultures is exemplified in Supplementary Figure S5. As P_{3A2} is not present in this pathway variant, R_{3A2} should not decrease deoxyviolacein production. In fact, deoxyviolacein production remains constant in the presence of R_{3A2} compared to the non-targeting control strain as expected and shown in Figure 8A, with a comparatively slight increase in prodeoxyviolacein production.

Finally, pathway variant 4 extends variant 3 by addition of P_{3A2}-driven *vioD*. As seen for pathway variant 2, inclusion of all five genes leads to accumulation of three metabolites, violacein, deoxyviolacein, and proviolacein, while R_{G6} again leads to near complete repression of all three compounds (Figure 8C and D). Although culture color differences are not as visually striking as in pathway variant 3, both R_{4A6} and R_{3A2} switches lead to significant attenuation of side products with concomitant increases in production of proviolacein and deoxyviolacein, respectively, of greater than ten-fold.

CONCLUSION

In this work, we present a method for rapid construction and screening of orthogonal dCas9–repressor promoter pairs for synthetic biology and metabolic engineering applications. Compared to the other methodologies presented to date, both of which maximize guide RNA:target DNA mismatches to force orthogonality, our strategy achieves mismatch-mediated orthogonality by introducing a small number of random PPSNR mismatches that also allow for exploration of the boundary between orthogonal and non-orthogonal promoter-repressor pairs. Although this proce-

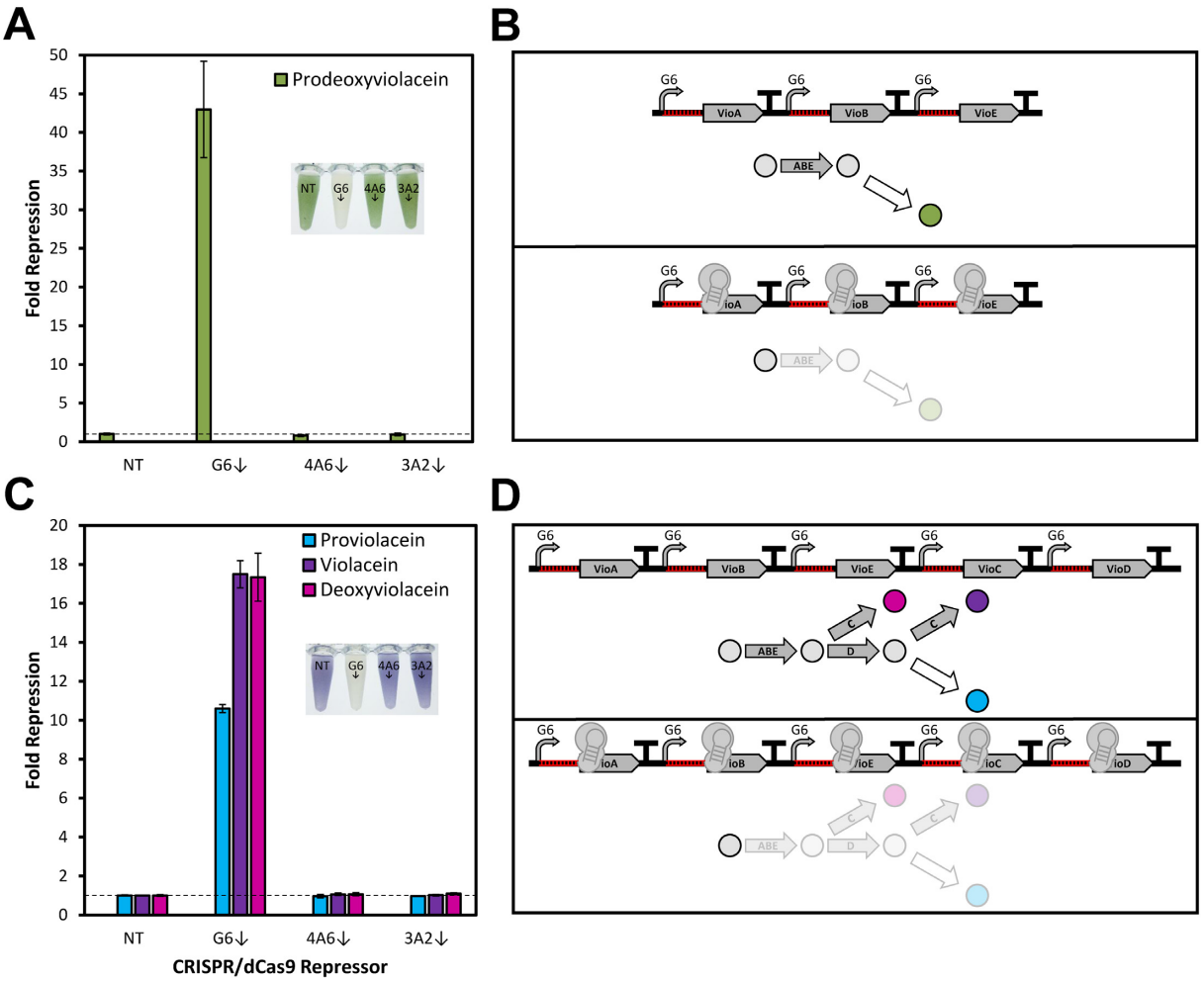

Figure 7. (**A**) Demonstration of orthogonality using minimal three gene VioABE pathway. (**B**) Minimal crosstalk by non-cognate repressors (top) and high repression fold change by cognate repressor R_{G6} (bottom) against G6-VioABE pathway generating prodeoxyviolacein. Faded pathway segments represent intended effect of dCas9-mediated repression. (**C**) Demonstration of orthogonality using full five-gene pathway G6-VioABECD. The three major metabolites of this pathway variant are not repressed by non-cognate repressors R_{4A6} or R_{3A2} (**D**, top), but they are strongly repressed by the cognate repressor R_{G6} (**D**, bottom). Values represent mean fold repression of biological triplicates, and error bars represent SEM ($n = 3$). Dashed lines in bar graphs represent baseline production for non-targeting control strain. Insets are photographs of representative induced *E. coli* cultures in presence of indicated repressor.

dure was developed using $P_{T7\text{-}lac}$, we anticipate that the protocol can be applied to any promoter of interest, in any host organism that is responsive to dCas9-mediated transcriptional regulation. If orthogonal promoters of similar strength are desired, a dCas9 operator could be placed immediately downstream of any promoter (rather than utilizing an existing operator within the promoter sequence) to limit the effect of PPSNR mutagenesis on promoter strength.

Advantages of our methodology include rapid library generation in a single site-directed mutagenesis step, followed by upfront screening of functional promoters possessing a useful range of de-repressed transcription strengths. This is analogous to the classic strategy of generating promoter strength libraries with site-directed mutagenesis, except it capitalizes on the introduced mutations to direct orthogonality between non-cognate dCas9 repressor sequences. As all steps in this screening process utilize standard techniques and equipment available to most laboratories, the whole procedure can be easily and cost-effectively reproduced by any researcher in less than three weeks and would thereby enable rapid expansion of the number of characterized orthogonal promoter-repressor sets available to the synthetic biology community. Furthermore, we anticipate that this methodology will facilitate high-throughput assessment of dCas9-mediated hybridization of mismatched RNA:DNA heteroduplexes *in vivo* that, when coupled with next generation sequencing and FACS, would generate very large datasets from which sequence-specific mismatch design principles could be more adequately garnered for *de novo* design of orthogonal promoters regulated by dCas9 and other inactivated CRISPR nucleases (46) and, potentially, for evasion of off-target Cas9-induced double stranded breaks (27).

Conversely, there are potential limitations with this methodology. Despite selecting only three PPSNR nu-

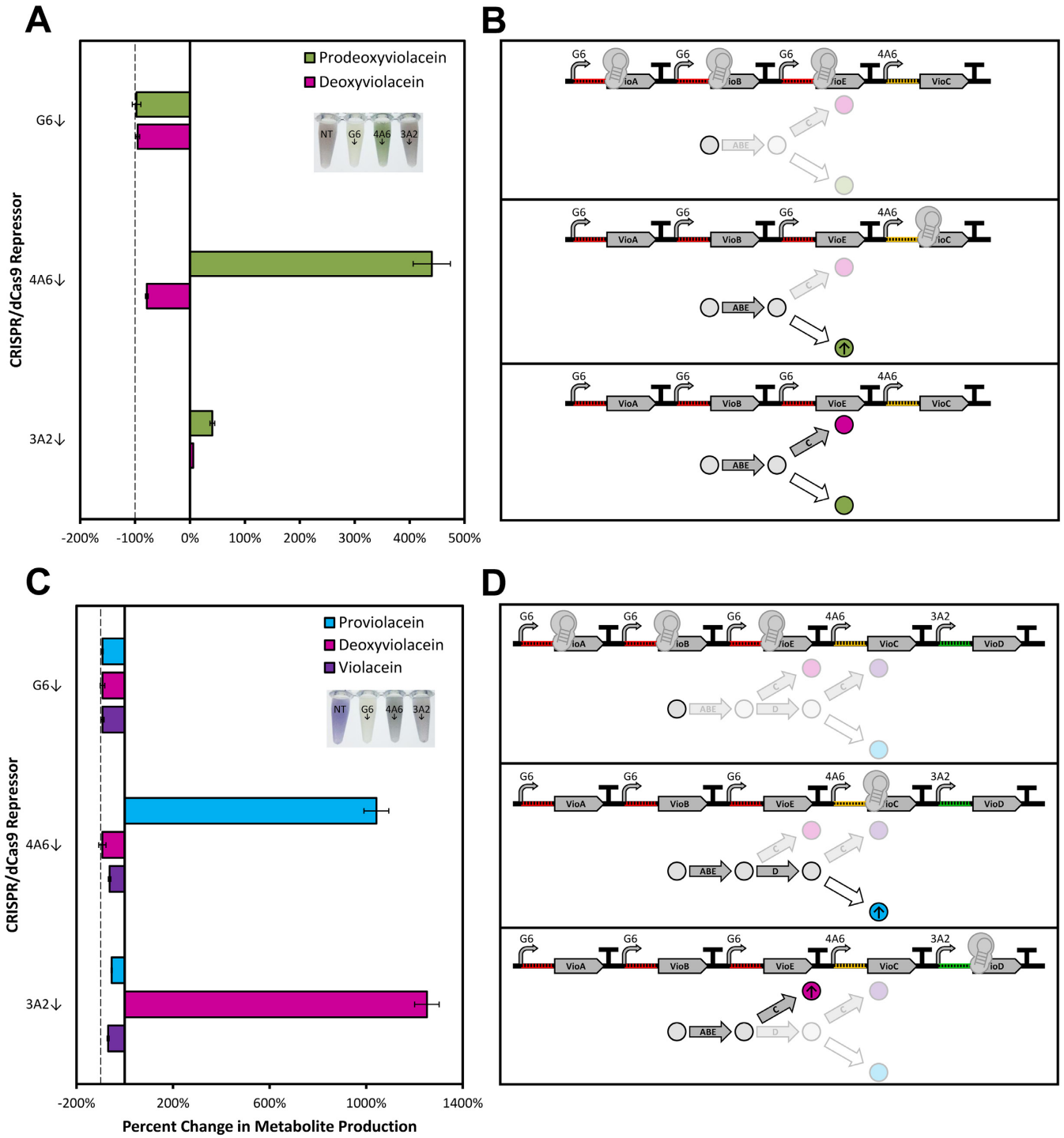

Figure 8. Orthogonal control over choice of natural product biosynthesis in *E. coli*. (**A**) Differential throttling and redirection of carbon flux using distinct dCas9 repressors against a single 4 gene pathway, G6-VioABE-4A6-VioC. (**B**) Nearly complete repression of both metabolites by R_{G6} (top), repression of deoxyviolacein and redirection toward prodeoxyviolacein by R_{4A6} repression of VioC (middle), and minimal change in production compared to non-targeting control using R_{3A2} in absence of P_{3A2} (bottom). (**C**) Dramatic reduction or diversion of metabolism with different dCas9 repressors against a single five-gene pathway, G6–VioABE–4A6–VioC–3A2–VioD. (**D**) Again, R_{G6} significantly represses production of all metabolites (top), while R_{4A6} drives carbon toward proviolacein (middle) and R_{3A2} increases production of prodeoxyviolacein by repression of VioD (bottom). Values represent mean fold repression of biological triplicates, and error bars represent SEM ($n = 3$). Dashed lines in bar graphs indicate complete repression. Insets are photographs of representative induced *E. coli* cultures in presence of indicated repressor.

cleotides for mutagenesis (discounting the single mutated nucleotide in the PAM since it does not affect orthogonality), the theoretical library size of sequences ($4^3 = 64$) and cognate/non-cognate promoter-spacer pairs ($64^2 = 4096$) generated by this strategy is much larger than most labs can realistically screen without robotic liquid handling instrumentation. However, by manually selecting promoters with useful expression levels upfront, many non-functional promoter sequences are likely culled from the library at this stage. As evidenced by this work, subsets of 5–10 orthogonal promoter-spacer pairs for use in modestly sized genetic circuits should nevertheless be readily attainable from a single round of screening 10–20 promoter-spacer pairs without appealing to liquid handlers. Additionally, mutagenesis library sizes could be constrained by intelligent primer design with mixed base degeneracy rather than complete A/T/C/G degeneracy, a strategy that might also deliberately bias libraries toward more orthogonal outcomes as design principles are realized. Finally, it is conceivable that layering of minimally mismatched orthogonal promoters in a genetic circuit might attenuate the repression capacity of cognate dCas9 repressors, since the increased number of similar but non-cognate promoter sequences could act as low-affinity, high-concentration decoys that partially sequester or titrate a repressor away from its cognate promoter (47). Until layering of these parts in higher order circuits has been addressed experimentally, however, we expect that such conveniently reconfigurable orthogonal promoters will be tremendously useful for construction of low-complexity circuits and development of functional tools with applications at the confluence of the fields of synthetic biology and metabolic engineering.

SUPPLEMENTARY DATA

Supplementary Data are available at NAR Online.

ACKNOWLEDGEMENTS

The authors would like to thank David Mathews for helpful discussions on RNA:DNA hybridization.
Author contributions: B.F.C., M.A.G.K., and R.J.L. designed the study, analyzed the data and wrote the manuscript. B.F.C. performed the experiments with assistance and advice from J.A.J., D.C.K., Q.D.L, J.A.E. and S.M.C. J.A.J. performed the initial mutant promoter strength screen.

FUNDING

Early-concept Grant for Exploratory Research (EAGER); National Science Foundation [MCB-1448657 to M.A.G.K.]. Funding for open access charge: National Science Foundation.
Conflict of interest statement. None declared.

REFERENCES

1. Cress,B.F., Trantas,E.A., Ververidis,F., Linhardt,R.J. and Koffas,M.A. (2015) Sensitive cells: enabling tools for static and dynamic control of microbial metabolic pathways. *Curr. Opin. Biotechnol.*, **36**, 205–214.
2. Blount,B.A., Weenink,T., Vasylechko,S. and Ellis,T. (2012) Rational diversification of a promoter providing fine-tuned expression and orthogonal regulation for synthetic biology. *PLoS One*, **7**, e33279.
3. Garg,A., Lohmueller,J.J., Silver,P.A. and Armel,T.Z. (2012) Engineering synthetic TAL effectors with orthogonal target sites. *Nucleic Acids Res.*, **40**, 7584–7595.
4. Lohmueller,J.J., Armel,T.Z. and Silver,P.A. (2012) A tunable zinc finger-based framework for Boolean logic computation in mammalian cells. *Nucleic Acids Res.*, **40**, 5180–5187.
5. Nielsen,A.A. and Voigt,C.A. (2014) Multi-input CRISPR/Cas genetic circuits that interface host regulatory networks. *Mol. Syst. Biol.*, **10**, 763.
6. Cress,B.F., Toparlak,Ö.D., Guleria,S., Lebovich,M., Stieglitz,J.T., Englaender,J.A., Jones,J.A., Linhardt,R.J. and Koffas,M.A.G. (2015) CRISPathBrick: modular combinatorial assembly of type II-A CRISPR arrays for dCas9-mediated multiplex transcriptional repression in E. coli. *ACS Synth. Biol.*, doi:10.1021/acssynbio.5b00012.
7. Zalatan,J.G., Lee,M.E., Almeida,R., Gilbert,L.A., Whitehead,E.H., La Russa,M., Tsai,J.C., Weissman,J.S., Dueber,J.E., Qi,L.S. *et al.* (2015) Engineering complex synthetic transcriptional programs with CRISPR RNA scaffolds. *Cell*, **160**, 339–350.
8. Farzadfard,F., Perli,S.D. and Lu,T.K. (2013) Tunable and multifunctional eukaryotic transcription factors based on CRISPR/Cas. *ACS Synth. Biol.*, **2**, 604–613.
9. Gilbert,L.A., Larson,M.H., Morsut,L., Liu,Z., Brar,G.A., Torres,S.E., Stern-Ginossar,N., Brandman,O., Whitehead,E.H., Doudna,J.A. *et al.* (2013) CRISPR-mediated modular RNA-guided regulation of transcription in eukaryotes. *Cell*, **154**, 442–451.
10. Didovyk,A., Borek,B., Hasty,J. and Tsimring,L. (2016) Orthogonal modular gene repression in Escherichia coli using engineered CRISPR/Cas9. *ACS Synth. Biol.*, **5**, 81–88.
11. Qi,L.S., Larson,M.H., Gilbert,L.A., Doudna,J.A., Weissman,J.S., Arkin,A.P. and Lim,W.A. (2013) Repurposing CRISPR as an RNA-guided platform for sequence-specific control of gene expression. *Cell*, **152**, 1173–183.
12. Larson,M.H., Gilbert,L.A., Wang,X., Lim,W.A., Weissman,J.S. and Qi,L.S. (2013) CRISPR interference (CRISPRi) for sequence-specific control of gene expression. *Nat. Protoc.*, **8**, 2180–1296.
13. Gilbert,L.A., Horlbeck,M.A., Adamson,B., Villalta,J.E., Chen,Y., Whitehead,E.H., Guimaraes,C., Panning,B., Ploegh,H.L., Bassik,M.C. *et al.* (2014) Genome-scale CRISPR-mediated control of gene repression and activation. *Cell*, **159**, 647–661.
14. Künne,T., Swarts,D.C. and Brouns,S.J.J. (2014) Planting the seed: target recognition of short guide RNAs. *Trends Microbiol.*, **22**, 74–83.
15. Jiang,F., Zhou,K., Ma,L., Gressel,S. and Doudna,J.A. (2015) A Cas9-guide RNA complex preorganized for target DNA recognition. *Science*, **348**, 1477–1481.
16. Conrad,B., Savchenko,R.S., Breves,R. and Hofemeister,J. (1996) A T7 promoter-specific, inducible protein expression system for Bacillus subtilis. *Mol. Gen. Genet.*, **250**, 230–236.
17. Müller,M., Ausländer,S., Ausländer,D., Kemmer,C. and Fussenegger,M. (2012) A novel reporter system for bacterial and mammalian cells based on the non-ribosomal peptide indigoidine. *Metab. Eng.*, **14**, 325–235.
18. Jones,J.A., Vernacchio,V.R., Lachance,D.M., Lebovich,M., Fu,L., Shirke,A.N., Schultz,V.L., Cress,B., Linhardt,R.J. and Koffas,M.A.G. (2015) ePathOptimize: a combinatorial approach for transcriptional balancing of metabolic pathways. *Sci. Rep.*, **5**, 11301.
19. Sanjana,N.E., Cong,L., Zhou,Y., Cunniff,M.M., Feng,G. and Zhang,F. (2012) A transcription activator-like effector toolbox for genome engineering. *Nat. Protoc.*, **7**, 171–192.
20. Bikard,D., Jiang,W., Samai,P., Hochschild,A., Zhang,F. and Marraffini,L.A. (2013) Programmable repression and activation of bacterial gene expression using an engineered CRISPR-Cas system. *Nucleic Acids Res.*, **41**, 7429–7437.
21. Xu,P., Vansiri,A., Bhan,N. and Koffas,M.A.G. (2012) ePathBrick: a synthetic biology platform for engineering metabolic pathways in E. coli. *ACS Synth. Biol.*, **1**, 256–266.
22. Temme,K., Hill,R., Segall-Shapiro,T.H., Moser,F. and Voigt,C.A. (2012) Modular control of multiple pathways using engineered orthogonal T7 polymerases. *Nucleic Acids Res.*, **40**, 8773–8781.

23. Davidson,E.A., VAN Blarcom,T., Levy,M. and Ellington,A.D. (2010) Emulsion based selection of T7 promoters of varying activity. *Pac. Symp. Biocomput.*, **443**, 433–443.
24. Biggs,B.W., Giaw,C., Sagliani,K., Shankar,S. and Stephanopoulos,G. (2016) Overcoming heterologous protein interdependency to optimize P450-mediated Taxol precursor synthesis in Escherichia coli. *Proc. Natl. Acad. Sci. U.S.A.*, doi:10.1073/pnas.1515826113.
25. Wu,G., Yan,Q., Jones,J.A., Tang,Y.J., Fong,S.S. and Koffas,M.A.G. (2016) Metabolic Burden: Cornerstones in Synthetic Biology and Metabolic Engineering Applications. *Trends Biotechnol.*, **xx**, 1–13.
26. Lin,Y., Cradick,T.J., Brown,M.T., Deshmukh,H., Ranjan,P., Sarode,N., Wile,B.M., Vertino,P.M., Stewart,F.J. and Bao,G. (2014) CRISPR/Cas9 systems have off-target activity with insertions or deletions between target DNA and guide RNA sequences. *Nucleic Acids Res.*, **42**, 7473–7485.
27. Kleinstiver,B.P., Pattanayak,V., Prew,M.S., Tsai,S.Q., Nguyen,N.T., Zheng,Z. and Joung,J.K. (2016) High-fidelity CRISPR-Cas9 nucleases with no detectable genome-wide off-target effects. *Nature*, doi:10.1038/nature16526.
28. Kuscu,C., Arslan,S., Singh,R., Thorpe,J. and Adli,M. (2014) Genome-wide analysis reveals characteristics of off-target sites bound by the Cas9 endonuclease. *Nat. Biotechnol.*, **32**, 677–683.
29. Josephs,E.A., Kocak,D.D., Fitzgibbon,C.J., McMenemy,J., Gersbach,C.A. and Marszalek,P.E. (2015) Structure and specificity of the RNA-guided endonuclease Cas9 during DNA interrogation, target binding and cleavage. *Nucleic Acids Res.*, doi:10.1093/nar/gkv1293.
30. Farasat,I. and Salis,H.M. (2016) A Biophysical Model of CRISPR/Cas9 Activity for Rational Design of Genome Editing and Gene Regulation. *PLOS Comput. Biol.*, **12**, e1004724.
31. SantaLucia,J. and Hicks,D. (2004) The thermodynamics of DNA structural motifs. *Annu. Rev. Biophys. Biomol. Struct.*, **33**, 415–440.
32. Kierzek,R., Burkard,M.E. and Turner,D.H. (1999) Thermodynamics of single mismatches in RNA duplexes. *Biochemistry*, **38**, 14214–14223.
33. Watkins,N.E., Kennelly,W.J., Tsay,M.J., Tuin,A., Swenson,L., Lee,H.-R., Morosyuk,S., Hicks,D.A. and Santalucia,J. (2011) Thermodynamic contributions of single internal rA·dA, rC·dC, rG·dG and rU·dT mismatches in RNA/DNA duplexes. *Nucleic Acids Res.*, **39**, 1894–1902.
34. Sugimoto,N., Nakano,M. and Nakano,S. (2000) Thermodynamics-structure relationship of single mismatches in RNA/DNA duplexes. *Biochemistry*, **39**, 11270–11281.
35. Lorenz,R., Hofacker,I.L. and Bernhart,S.H. (2012) Folding RNA/DNA hybrid duplexes. *Bioinformatics*, **28**, 2530–2531.
36. Brewster,R.C., Weinert,F.M., Garcia,H.G., Song,D., Rydenfelt,M. and Phillips,R. (2014) The transcription factor titration effect dictates level of gene expression. *Cell*, **156**, 1312–1323.
37. Segall-Shapiro,T.H., Meyer,A.J., Ellington,A.D., Sontag,E.D. and Voigt,C.A. (2014) A 'resource allocator' for transcription based on a highly fragmented T7 RNA polymerase. *Mol. Syst. Biol.*, **10**, 742.
38. Brophy,J.A.N. and Voigt,C.A. (2014) Principles of genetic circuit design. *Nat. Methods*, **11**, 508–520.
39. Nielsen,A.A.K., Segall-Shapiro,T.H. and Voigt,C.A. (2013) Advances in genetic circuit design: novel biochemistries, deep part mining, and precision gene expression. *Curr. Opin. Chem. Biol.*, **17**, 878–892.
40. Stanton,B.C., Nielsen,A.A.K., Tamsir,A., Clancy,K., Peterson,T. and Voigt,C.A. (2013) Genomic mining of prokaryotic repressors for orthogonal logic gates. *Nat. Chem. Biol.*, doi:10.1038/nchembio.1411.
41. Jones,J.A., Toparlak,Ö.D. and Koffas,M.A.G. (2015) Metabolic pathway balancing and its role in the production of biofuels and chemicals. *Curr. Opin. Biotechnol.*, **33**, 52–59.
42. Torella,J.P., Boehm,C.R., Lienert,F., Chen,J.-H., Way,J.C. and Silver,P.A. (2014) Rapid construction of insulated genetic circuits via synthetic sequence-guided isothermal assembly. *Nucleic Acids Res.*, **42**, 681–689.
43. Lee,M.E., Aswani,A., Han,A.S., Tomlin,C.J. and Dueber,J.E. (2013) Expression-level optimization of a multi-enzyme pathway in the absence of a high-throughput assay. *Nucleic Acids Res.*, **41**, 10668–10678.
44. Mitchell,L.A., Chuang,J., Agmon,N., Khunsriraksakul,C., Phillips,N.A., Cai,Y., Truong,D.M., Veerakumar,A., Wang,Y., Mayorga,M. *et al.* (2015) Versatile genetic assembly system (VEGAS) to assemble pathways for expression in S. cerevisiae. *Nucleic Acids Res.*, **43**, 6620–6630.
45. Guo,Y., Dong,J., Zhou,T., Auxillos,J., Li,T., Zhang,W., Wang,L., Shen,Y., Luo,Y., Zheng,Y. *et al.* (2015) YeastFab: the design and construction of standard biological parts for metabolic engineering in Saccharomyces cerevisiae. *Nucleic Acids Res.*, **43**, e88.
46. Luo,M.L., Mullis,A.S., Leenay,R.T. and Beisel,C.L. (2014) Repurposing endogenous type I CRISPR-Cas systems for programmable gene repression. *Nucleic Acids Res.*, doi:10.1093/nar/gku971.
47. Sternberg,S.H., Redding,S., Jinek,M., Greene,E.C. and Doudna,J.A. (2014) DNA interrogation by the CRISPR RNA-guided endonuclease Cas9. *Nature*, **507**, 62–67.